RSC Advances

PAPER

View Article Online
View Journal | View Issue

Cite this: *RSC Adv.*, 2022, **12**, 19406

Oriented self-assembly of metal–organic frameworks driven by photoinitiated monomer polymerization†

Fuqiang Fan, * Zhihui Zhang, Qingqi Zeng, Liying Zhang, Xuemin Zhang, Tieqiang Wang and Yu Fu *

Received 19th May 2022
Accepted 29th June 2022

DOI: 10.1039/d2ra03161b

rsc.li/rsc-advances

The self-assembly of metal–organic frameworks (MOFs) is crucial for the functional design of materials, including energy storage materials, catalysts, selective separation materials and optical crystals. However, oriented self-assembly of MOFs is still a challenge. Herein, we propose a novel strategy to drive oriented self-assembly of MOF polyhedral particles at the water–liquid interface by photoinitiated monomer polymerization. The MOF polyhedral particles self-assemble into ordered close-packed structures with obvious orientation in the polymer film, and the orientation is determined by the casting solvent on the water surface. The prepared large-area MOF polymer films show a Janus structure, containing a MOF monolayer and a polymer layer, and can be easily transferred to a variety of substrates. In addition, mixed MOF particles with different sizes and morphologies can also be assembled by this method. This novel method can be foreseen to provide a powerful driving force for the development of MOF self-assembly and to create more possibilities for utilizing the anisotropic properties of MOFs.

Introduction

Metal–organic frameworks (MOFs), also known as crystalline polyhedral particles, possess anisotropic pore structures along different crystal facets and show special physicochemical properties depending on the crystallographic direction.[1–6] Recently, the fabrication of oriented MOFs has attracted increasing attention due to their applications in selective separation, catalysis, optical equipment and energy storage.[7–16] To achieve oriented growth of MOFs, most studies focused on the surface functionalization of substrates or crystal engineering.[17–22] However, these methods can only be used to fabricate single-type MOFs considering lattice matching, and the preparation process is complex and time-consuming, further limiting their versatility.

Self-assembly is a universal strategy to control the alignment of building blocks, which is an ideal candidate for the fabrication of oriented MOFs. It has been widely used in constructing superstructures of inorganic polyhedral nanoparticles (NPs) or polymer colloidal particles.[23–33] Regretfully, rapid progress in the self-assembly of inorganic NPs did not promote the development of MOFs in this field. Assembling MOFs into superstructures is promising in chemistry and materials science.[34–38] However, only a few studies have used MOFs as building blocks to construct multidimensional superstructures, and oriented MOF assemblies are even less common. For example, focused on 3D assembly, Maspoch *et al.* reported the self-assembly of MOFs and the assembly of MOFs with colloidal particles into ordered superstructures;[39,40] Yu and coworkers synthesized multiple types of ternary MOF-on-MOF heterostructures *via* a selective assembly strategy.[41] In contrast, 2D assembly tends to fabricate oriented MOF materials. For example, Shi *et al.* synthesized oriented MOF films by air–liquid interfacial assembly.[42] However, the method is applicable only to flat MOF nanosheets and not to other polyhedral particles. Cohen and coworkers fabricated MOF monolayer at the air–liquid interface using polymer-brush-coated MOF polyhedral particles.[43,44] Very recently, they proposed a novel method to control the 2D alignment of MOF polyhedral particles in polydimethylsiloxane (PDMS) films, which was achieved by casting different solvents, including a dispersed MOF and heat-curable PDMS, to immobilize the MOF particles at the water–liquid interface.[45] Although this work is inspiring and encouraging, heat as the reaction condition is relatively single and limited. By comparison, light as a stimulus resource has some unique advantages, such as high spatial and temporal resolution, variable tunable parameters, and different light sources. Using light as the stimulus to drive the self-assembly of MOFs will surely bring new breakthroughs to the development of MOF assemblies.

Herein, we selected a light-responsive monomer to drive oriented self-assembly of MOFs at water–liquid interfaces *via* photoinitiated ring-opening polymerization of the monomers (Scheme 1). To prove the universality of this method, two types

Department of Chemistry, College of Sciences, Northeastern University, Shenyang, 110819, PR China. E-mail: fanfuqiang@mail.neu.edu.cn; fuyu@mail.neu.edu.cn

† Electronic supplementary information (ESI) available. See https://doi.org/10.1039/d2ra03161b

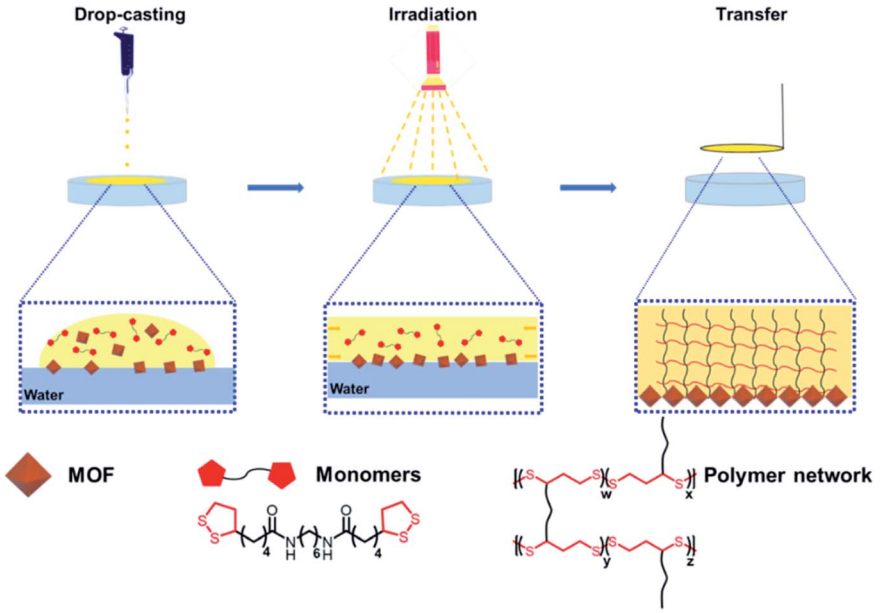

Scheme 1 Illustration of the preparation of oriented MOF polymer films.

of MOF polyhedral particles (MIL-96 and UIO-66) and three kinds of morphologies (spindle, hexagonal bifrustum, and octahedral) were used. The resulting films have a Janus structure, containing a MOF monolayer and a polymer layer, and the alignment of MOF particles in the films is close-packed and oriented. Notably, the orientation of the MOF polyhedral particles in the film depends on the water–liquid interface environment created by the casting solvents. In addition, mixed MOF particle polymer films can also be prepared by this method. Notably, this is an effective strategy for driving MOF self-assembly by simple light illumination without complex surface modification.

Results and discussion

Fabrication of oriented MOF films

Oriented MOF films were synthesized by a conventional drop-casting method. Briefly, the solution containing dispersed MOF polyhedral particles and photoresponsive monomer was carefully dropped onto a water surface and immediately illuminated using portable UV light. As the monomer polymerization, MOF polyhedral particles self-assemble into oriented MOF polymer films at the water–air interface. The process was first implemented using CH_2Cl_2 as the casting solvent. The synthetic film was transferred to a silicon wafer *via* a stamping operation, and characterized by scanning electron microscopy (SEM), atomic force microscope (AFM) and Fourier-transform infrared (FT-IR). Compared with random MOF particles, the particles in the film assembled into ordered close-packed structures with obvious orientations (Fig. 1 and S1†). The orientation corresponding to the <hkl> direction of MOFs was verified by powder X-ray diffraction (PXRD). For MIL-96, the orientation of the polyhedral particles was related to the morphology. The MIL-96 particles with the spindle morphology aligned parallel to their long axis, corresponding to the <200> orientation, and the peak of the <102> crystal plane disappeared (Fig. 1a, h and S2a†). In the term of hexagonal bifrustum, MIL-96 kept the trapezoid facet as the main crystal plane, corresponding to the <102> orientation (Fig. 1b, i and S2b†). For octahedral UIO-66, the particles aligned along the triangular facet, corresponding to the <111> orientation, and the peak of the <200> crystal plane disappeared (Fig. 1c, j and S2c†). Furthermore, the PXRD measurements and crystallographically preferred orientation (CPO) index quantifying the degree of crystal orientation verified the strong orientation of MOFs in the polymer films (Table S1†). The IR spectrum shown the films were composed of disulfide polyurethane and MOF particles (Fig. S3†).

Interestingly, different from the mixed MOF polymer membrane, the prepared MOF polymer films have a Janus structure. As shown in the cross-section SEM images, the polymer layer is present over the monolayer of MOF particles (Fig. 1d–f). This means that the MOF polyhedral particles self-assembled at the water–solvent interface and the monomers polymerized at the solvent–air interface. The synthesized MOF polymer film could achieve a size of nearly 24 cm^2, and the MOF polyhedral particles in the film were uniform across the whole film, which was demonstrated by SEM images sampled at three different locations in the film (Fig. S4†). In addition, the MOF polymer film is freestanding and easily be transferred to other substrates (Fig. S5†).

Controllable orientation of MOFs assembly by casting solvents

To explore the reason for the oriented self-assembly, multiple solvents with different parameters (including polarity, vapor pressure, density, interfacial tension) were used as the casting solvent to prepare the MOF films (Table S2†). As shown in Fig. 2,

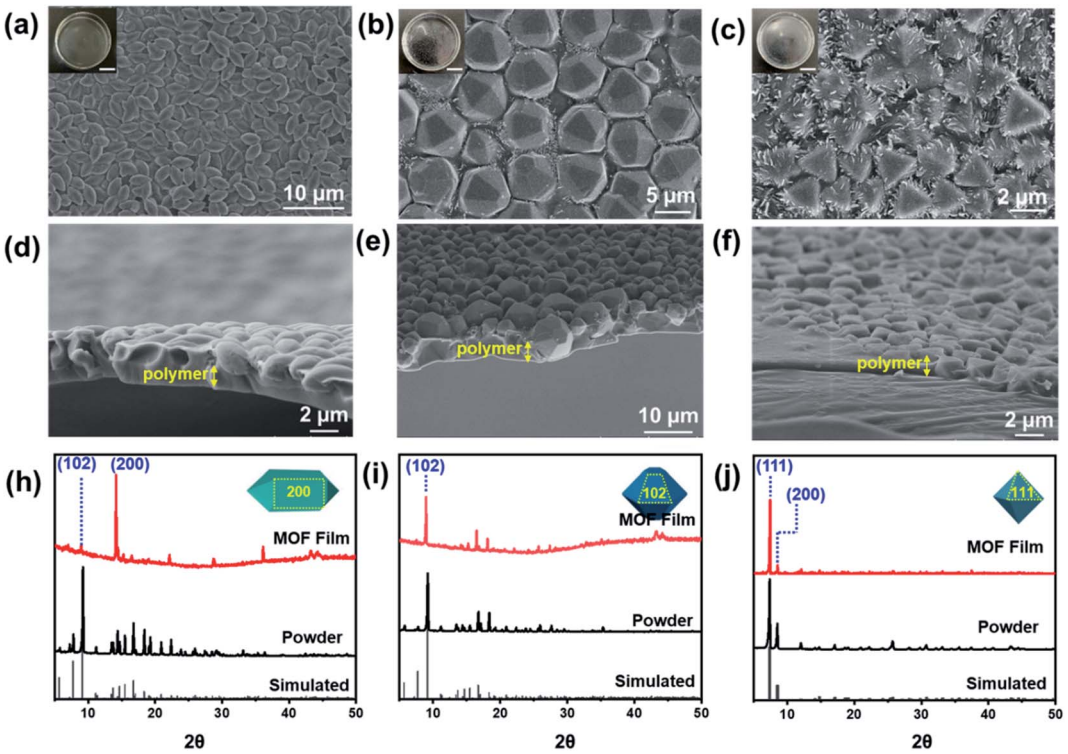

Fig. 1 SEM images and PXRD patterns of the bottom surface of MOF polymer films prepared using different MOF particles with CH_2Cl_2 as the casting solvent. (a, d and h) Spindle morphology of MIL-96; (b, e and i) hexagonal bifrustum morphology of MIL-96; (c, f and j) octahedral morphology of UIO-66. The scale bar in the insert is 2 cm.

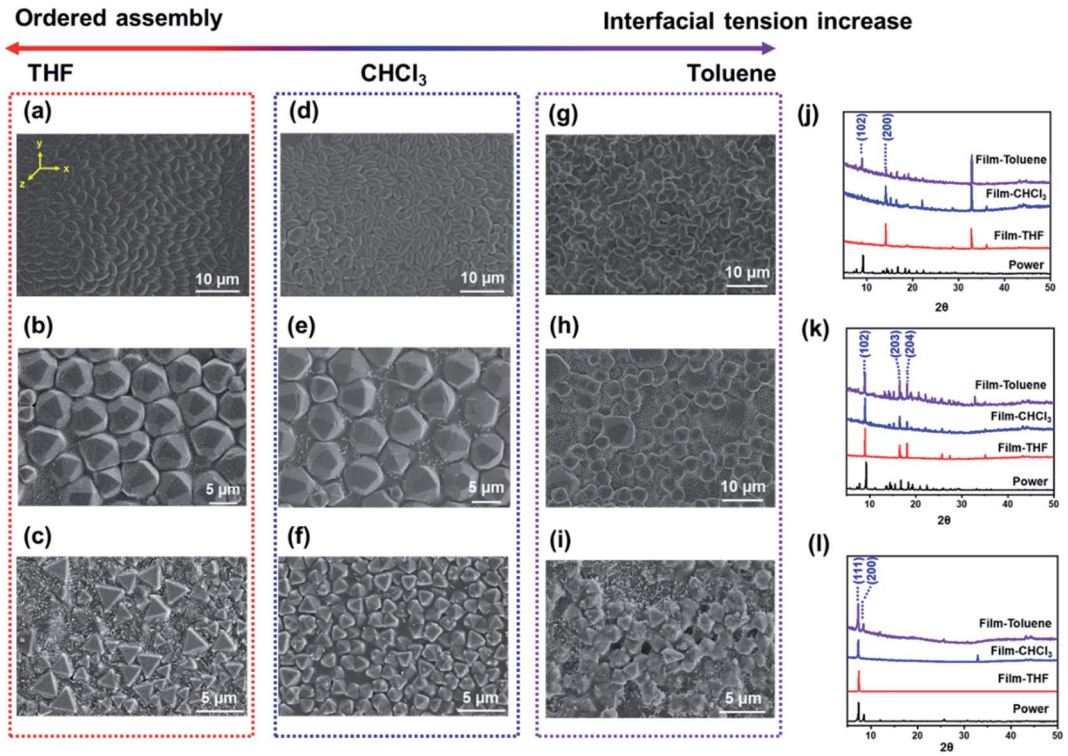

Fig. 2 SEM images of the bottom surface of the MIL-96 spindle morphology, MIL-96 hexagonal bifrustum morphology, and UIO-66 octahedral morphology films prepared using different solvents: (a–c) THF; (d–f) $CHCl_3$; (g–i) toluene. PXRD patterns of the films obtained using different MOF and solvents: (j) MIL-96 spindle morphology, (k) MIL-96 hexagonal bifrustum morphology, and (l) UIO-66 octahedral morphology films.

the orientation of the MOF in the film is related with the interfacial tension of the casting solvent. For solvents that are miscible with water, such as tetrahydrofuran (THF) or dimethyl sulfoxide (DMSO), MOF particles self-assembled into ordered close-packed structures and showed a uniform crystal plane orientation at the water–solvent interface (*x*-axis and *y*-axis) (Fig. 2a–c and S6a–c†). Note that when DMSO was used as the casting solvent, the polymer layer nearly covered the MOF layer. This might be because DMSO is heavier than water; when the casting solvent was dropped on the water interface, DMSO rapidly diffused, resulting in the MOF layer being completely coated in the polymer film. With increasing interfacial tension of the casting solvent, such as ethyl acetate (EAC) or $CHCl_3$, the assembly of MOF particles showed aggregation along the *z*-axis direction, which disturbed the long-range order of the assembly at the water–liquid interface (Fig. 2d–f and S6d–f†). In terms of using casting solvents with higher interfacial tension, such as toluene, the MOF particles in the film showed random packing (Fig. 2g–i). PXRD measurements and CPO index further verified the change in the crystal orientation of the MOF films with the casting solvent (Fig. 2j–l and Table S3†). Based on the results, a possible assembly process of the MOF particles is deduced. When solvents are miscible with water or have a low interfacial tension, they can quickly spread on the water interface after drop casting. During the polymerization of the monomers, a shrinkage force is generated and acts on the MOF particles, guiding the assembly. As the interfacial tension of the casting solution increases, the solution cannot completely spread on the water interface, resulting in aggregation of the MOF assembly (Fig. S7†). Thus, the self-assembly of MOF polyhedral particles is driven by the photoinitiated monomer polymerization, and the oriented assembly of the MOF particles is dependent on the interfacial tension of the casting solvent.

Fabrication of MOF films under visible light

Because the self-assembly of the MOF particles is driven by the shrinkage force of the monomer polymerization, some factors that might affect the polymerization were also discussed, such as the light source and light intensity. The oriented assembly of the MOF particles could also be driven by irradiation of visible light, and the alignment of the MOF particles in the film was similar with that under UV light. Furthermore, the light intensity showed no correlation with the alignment of the MOF particles in the polymer film (Fig. S8†).

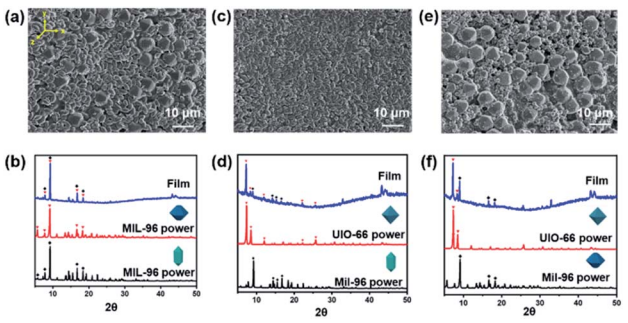

Fig. 3 SEM images and PXRD patterns of the mixed MOF films prepared using CH_2Cl_2 as the casting solvent: (a and b) MIL-96 spindle morphology and hexagonal bifrustum morphology film; (c and d) MIL-96 spindle morphology and UIO-66 octahedral morphology film; (e and f) MIL-96 hexagonal bifrustum morphology and UIO-66 octahedral morphology film.

Fabrication of mixed MOF particles films

Assembly of mixed MOF particles was also implemented. The spindle MIL-96 (4 μm) and octahedral UIO-66 (1 μm) with similar morphologies assembled into a close-packing arrangement, while the hexagonal bifrustum MIL-96 (6 μm) and octahedral UIO-66 (1 μm) with greater size and morphology differences resulted in gaps and aggregates in the film (Fig. 3). This might be because the difference in size and morphology of the MOF particles resulted in inconsistent direction of the shrinkage force that acted on them. The greater the size difference of the mixed MOF particles, the more particles aggregated in the *z*-axis direction, and more gaps appeared in the film.

Conclusions

In summary, a novel strategy capable of driving oriented self-assembly of MOF polyhedral particles at the water–liquid interface by photoinitiated monomer polymerization has been proposed. The synthesized MOF film has a Janus structure and can be transferred to various substrates. The alignment of the MOF particles in the polymer film is close-packed and highly oriented. In addition, mixed MOF polymer films can also be prepared by this method. This work can be foreseen to accelerate the development of MOF assemblies and provide a novel strategy for utilizing the anisotropic properties of MOFs.

Experimental

Materials and instrumentation

DL-thioctic acid, 1,6-hexamethylene diisocyanate (HDI), and dibutyltin dilaurate were purchased from J&K Scientific, Beijing, China. Aluminum nitrate nonahydrate, 1,3,5-benzentricarboxylic acid, terephthalic acid, and zirconium(IV) chloride were obtained from Macklin, Beijing, China. Other reagents and solvents were purchased from Sinopharm Chemical Reagent Co., Ltd. All reagents and solvents were used without further purification. A xenon light source was obtained from Shanghai Jiguang Special Lighting Co. Ltd. Imagines of the product were collected by field-emission SEM (FE-SEM, Hitachi SU8010). PXRD data were collected on a diffractometer equipped with a Cu Kα radiation source ($\lambda = 1.5406$ Å).

Synthesis of UIO-66

Octahedral UIO-66 was synthesized according to a previous study.[46] Briefly, $ZrCl_4$ (0.14 g, 0.601 mmol) and terephthalic acid (0.1 g, 0.602 mmol) were dissolved in 20 mL of dimethylformamide (DMF) by ultrasonication for 10 minutes, and then, 2.774 mL of glacial acetic acid was added. The white

solution was transferred to a 100 mL Teflon kettle and heated to 120 °C for 24 hours. After cooling to room temperature, the white powder was washed 3 times with DMF and methanol each.

Synthesis of MIL-96

The MIL-96 particles with the spindle morphology and hexagonal bifrustum morphology were prepared according to a previous study.[47] For hexagonal bifrustum MIL-96, $Al(NO_3)_3 \cdot 9H_2O$ (1.5 g, 4 mmol) and 1,3,5-benzentricarboxylic acid (0.84 g, 4 mmol) were dissolved in 18 mL of a mixture of DMF and H_2O in a 1 : 4 volumetric ratio (v/v), and then, 2.28 mL of glacial acetic acid was added. The mixture solution was transferred to a 100 mL Teflon kettle and heated 130 °C for 24 h. After cooling, the white powder was washed 3 times with DMF and methanol each. Similarly, spindle MIL-96 was synthesized with a 1 : 4 ratio of the THF : H_2O mixture.

Preparation of orientated MOF films

100 mg of DL-thioctic acid was dissolved in 0.5 mL of casting solvent in a vial; then, 25 μL of HDI and 10 μL of dibutyltin dilaurate were added, and the vial was shaken for 5 minutes. After that, different MOF particles (5 mg for UIO-66, 10 mg for MIL-96) were dispersed in 100 μL of this solution. 25 μL of the casting solution was carefully dropped on a water surface and immediately irradiated by a portable ultraviolet lamp for 10 minutes.

Author contributions

F. Q. Fan and Y. Fu designed the concept of the work. F. Q. Fan, Z. H. Zhang and Q. Q. Zeng performed the major experiments. L. Y. Zhang, X. M. Zhang and T. Q. Wang analyzed the data. All authors have given approval to the final version of the manuscript.

Conflicts of interest

There are no conflicts to declare.

Acknowledgements

This work was supported by the National Natural Science Foundation of China (22175030, 22175031, 22101042, 22075039), Project funded by China Postdoctoral Science Foundation (2020M670773), the Open Project of State Key Laboratory of Supramolecular Structure and Materials (sklssm202205, sklssm2022020). Special thanks are due to the instrumental from Analytical and Testing Center, Northeastern University.

Notes and references

1 W. T. Xu, B. B. Tu, Q. Liu, Y. F. Shu, C. C. Liang, C. S. Diercks, O. M. Yagi, Y. B. Zhang, H. X. Deng and Q. W. Li, *Nat. Rev.*, 2020, **5**, 765–779.
2 H. Furukawa, K. E. Cordova, M. O'Keeffe and O. M. Yaghi, *Science*, 2013, **341**, 1230444.
3 Z. Ji, H. Z. Wang, S. Canossa, S. Wuttke and O. M. Yaghi, *Adv. Funct. Mater.*, 2020, **30**, 2000238.
4 S. Yuan, L. Feng, K. C. Wang, J. D. Pang, M. Bosch, C. Lollar, Y. J. Sun, J. S. Qin, X. Y. Yang, P. Zhang, Q. Wang, L. F. Zou, Y. M. Zhang, L. L. Zhang, Y. Fang, J. L. Li and H.-C. Zhou, *Adv. Mater.*, 2018, **30**, 1704303.
5 N. S. Bobbitt, M. L. Mendonca, A. Howarth, T. Islamoglu, J. T. Hupp, O. K. Farha and R. Q. Snurr, *Chem. Soc. Rev.*, 2017, **46**, 3357–3385.
6 S. Z. Cong, Y. Yuan, J. X. Wang, Z. Zhang, F. Kapteijn and X. L. Liu, *J. Am. Chem. Soc.*, 2021, **143**, 20055–20058.
7 X. J. Bai, X. Zhai, L. Y. Zhang, Y. Fu and W. Qi, *Matter*, 2021, **4**, 2919–2935.
8 X. F. Shi, Y. L. Xu, B. Zhao, P. P. Li, M. Song, J. J. Jia, H. J. Yu and G. Lu, *Adv. Mater. Interfaces*, 2021, **8**, 2100586.
9 X. L. Zhou, H. Y. Jin, B. Y. Xia, K. Davey, Y. Zheng and S.-Z. Qiao, *Adv. Mater.*, 2021, 2104341.
10 P. B. Geng, L. Wang, M. Du, Y. Bai, W. T. Li, Y. F. Liu, S. Q. Chen, P. Braunstein, Q. Xu and H. Pang, *Adv. Mater.*, 2022, **34**, 2107836.
11 T. Deng, Y. Lu, W. Zhang, M. L. Sui, X. Y. Shi, D. Wang and W. T. Zheng, *Adv. Energy Mater.*, 2018, **8**, 1702294.
12 S. M. Yoon, J. H. Park and B. A. Grzybowski, *Angew. Chem., Int. Ed.*, 2017, **129**, 133–138.
13 Y. Shen, T. Pan, L. Wang, Z. Ren, W. N. Zhang and F. W. Huo, *Adv. Mater.*, 2021, **33**, 2007442.
14 P. P. Zhang, X. Q. Zou, J. Song, Y. Y. Tian, Y. L. Zhu, G. L. Yu, Y. Yuan and G. S. Zhu, *Adv. Mater.*, 2020, **32**, 107449.
15 L. L. Wang, C. Zeng, H. Xu, P. C. Yin, D. C. Chen, J. Deng, M. Li, N. Zheng, C. Gu and Y. G. Ma, *Chem. Sci.*, 2019, **10**, 1023–1028.
16 C. Gu, N. Hosono, J.-J. Zheng, Y. Sato, S. Kusaka, S. Sakaki and S. Kitagawa, *Science*, 2019, **363**, 387–391.
17 W. Yang, H. J. Wang, R. R. Liu, J. W. Wang, C. Zhang, C. Li, D. C. Zhong and T. B. Lu, *Angew. Chem., Int. Ed.*, 2021, **60**, 409–414.
18 A. S. Deng, X. T. Shen, Z. Wan, Y. H. Li, S. Y. Pang, X. He, J. Caro and A. S. Huang, *Angew. Chem., Int. Ed.*, 2021, **60**, 25463–25467.
19 E. Biemmi, C. Scheerb and T. Bein, *J. Am. Chem. Soc.*, 2007, **129**, 8054–8055.
20 L. Wang, J. W. Wan, Y. S. Zhao, N. L. Yang and D. Wang, *J. Am. Chem. Soc.*, 2019, **141**, 2238–2241.
21 X. X. Ma, Z. Wan, Y. H. Li, X. He, J. Caro and A. S. Huang, *Angew. Chem., Int. Ed.*, 2020, **59**, 20858–20862.
22 P. Falcaro, K. Okada, T. Hara, K. Ikigaki, Y. Tokudome, A. W. Thornton, A. J. Hill, T. Williams, C. Doonan and M. Takahashi, *Nat. Mater.*, 2017, **16**, 342–349.
23 D. Jung, C. Lim, H. J. Shim, Y. Kim, C. Park, J. Jung, S. I. Han, S.-H. Sunwoo, K. W. Cho, G. D. Cha, D. C. Kim, J. H. Koo, J. H. Kim, T. Hyeon and D.-H. Kim, *Science*, 2021, **373**, 1022–1026.
24 C. K. Song, B. Y. Ye, J. Y. Xu, J. H. Chen, W. Shi, C. P. Yu, C. W. An, J. W. Zhu and W. C. Zhang, *Small*, 2021, 2104202.

25 J. W. Lv, X. Q. Gao, B. Han, Y. F. Zhu, K. Hou and Z. Y. Tang, *Nat. Rev. Chem.*, 2022, **6**, 125–145.
26 L. R. Macfarlane, H. Shaikh, J. D. Garcia-Hernandez, M. Vespa, T. Fukui and I. Manners, *Nat. Rev. Mater.*, 2021, **6**, 7–26.
27 C. Li, Q. Li, Y. V. Kaneti, D. Hou, Y. Yamauchi and Y. Y. Mai, *Chem. Soc. Rev.*, 2020, **49**, 4681–4736.
28 Y. T. Sang and M. H. Liu, *Chem. Sci.*, 2022, **13**, 633–656.
29 T. Bian, A. Gardin, J. Gemen, L. Houben, C. Perego, B. Lee, N. Elad, Z. Chu, G. M. Pavan and R. Klajn, *Nat. Chem.*, 2021, **13**, 940–949.
30 P. J. Santos, P. A. Gabrys, L. Z. Zornberg and M. S. Lee, *Nature*, 2021, **591**, 586–591.
31 Q. Li, J. C. Russell, T. Y. Luo, X. Roy, N. L. Rosi, Y. Zhu and R. C. Jin, *Nat. Commun.*, 2018, **9**, 3871–3878.
32 H. Liu, H. G. Wang, Q. Song, K. Küster, U. Starke, P. A. van Aken and E. Klemm, *Angew. Chem., Int. Ed.*, 2022, **61**, 20211058.
33 W. Cao and H. P. Xu, *Mater. Chem. Front.*, 2019, **3**, 2010–2017.
34 H. B. Zou, J. Y. Dai, J. Q. Suo, R. Ettelaie, Y. Li, N. Xue, R. W. Wang and H. Q. Yang, *Nat. Commun.*, 2021, **12**, 4968–4979.
35 J. W. Wang, Y. Liu, G. Bleyer, E. S. A. Goerlitzer, S. Englisch, T. Przybilla, C. F. Mbah, M. Engel, E. Spiecker, I. Imaz, D. Maspoch and N. Vogel, *Angew. Chem., Int. Ed.*, 2022, e202117455.
36 J. M. Guo, Y. L. Yu, W. Zhu, R. E. Serda, S. Franco, L. Wang, Q. Lei, J. O. Agola, A. Noureddine, E. Ploetz, S. Wuttke and C. J. Brinker, *Adv. Funct. Mater.*, 2021, **31**, 2005935.
37 Y. Jiang, X. Pan, M. Yao, L. Han, X. Zhang, Z. Jia, J. Weng, W. Chen, L. Fang, X. Wang, Y. Zhang, R. Duan, F. Ren, K. Wang, X. Chen and X. Lu, *Nanotoday*, 2021, **39**, 101182.
38 Y. X. Shi, Y. Wu, S. Q. Wang, Y. Y. Zhao, T. Li, X. Q. Yang and T. Zhang, *J. Am. Chem. Soc.*, 2021, **143**, 4017–4023.
39 C. Avci, I. Imaz, A. Carné-Sánchez, J. A. Pariente, N. Tasios, J. Pérez-Carvajal, M. I. Alonso, A. Blanco, M. Dijkstra, C. López and D. Maspoch, *Nat. Chem.*, 2018, **10**, 78–84.
40 Y. Liu, J. M. Wang, I. Imaz and D. Maspoch, *J. Am. Chem. Soc.*, 2021, **143**, 12943–12947.
41 C. Liu, Q. Sun, L. N. Lin, J. Wang, C. Q. Zhang, C. H. Xia, T. Bao, J. J. Wan, R. Huang, J. Zou and C. Z. Yu, *Nat. Commun.*, 2020, **11**, 4971–4979.
42 N. E. Shi, J. Zhang, Z. Ding, H. Jiang, Y. Yan, D. Q. Gu, W. Li, M. D. Yi, F. Z. Huang, S. F. Chen, L. H. Xie, Y. B. Ren, Y. Li and W. Huang, *Adv. Funct. Mater.*, 2021, 2110784.
43 Y. Katayama, M. Kalaj, K. S. Barcus and S. M. Cohen, *J. Am. Chem. Soc.*, 2019, **141**, 20000–20003.
44 K. Barcus and S. M. Cohen, *Chem. Sci.*, 2020, **11**, 8433–8437.
45 J. Y. Kim, K. Barcus and S. M. Cohen, *J. Am. Chem. Soc.*, 2021, **143**, 3703–3706.
46 Y. Zhao, Q. Zhang, Y. Li, R. Zhang and G. Lu, *ACS Appl. Mater. Interfaces*, 2017, **9**, 15079–15085.
47 M. Sindoro, A. Y. Jee and S. Granick, *Chem. Commun.*, 2013, **49**, 9576–9578.